

## Article

# Effectiveness of Noble Gas Addition for Plasma Synthesis of Ammonia in a Dielectric Barrier Discharge Reactor

Yihao Xu <sup>1</sup>, Hao Yuan <sup>2</sup>, Hongli Wang <sup>2</sup>, Ke Lu <sup>2</sup> and Dezheng Yang <sup>1,2,\*</sup><sup>1</sup> College of Sciences, Shihezi University, Shihezi 832003, China; 20212018006@stu.shzu.edu.cn<sup>2</sup> Key Lab of Materials Modification by Laser, Ion, and Electron Beams, Dalian University of Technology, Ministry of Education, Dalian 116024, China; yuanhao@dlut.edu.cn (H.Y.); wanghongli110@mail.dlut.edu.cn (H.W.); lukelo0k@mail.dlut.edu.cn (K.L.)

\* Correspondence: yangdz@dlut.edu.cn; Tel.: +86-13322214836

**Abstract:** Non-thermal plasma driven ammonia synthesis has great potential for future industrial applications due to its low theoretical energy requirements. To achieve technological advancement and environmental sustainability, it is crucial to boost the energy yield in plasma-assisted ammonia synthesis. Therefore, optimizing energy transfer and utilization are key strategies for enhancing energy efficiency. In this study, dielectric barrier discharge driven by a nanosecond pulsed power supply is used to enhance plasma-assisted ammonia synthesis by controlling the energy transfer through the addition of noble gases. It was found that the addition of noble gases changed the plasma characteristics, significantly improved the uniformity of the discharge, and achieved a high energy yield for ammonia synthesis. The effects of additive amounts of argon (Ar) and helium (He), as well as the pulse parameters including the pulse voltage, pulse repetition frequency, pulse width, and pulse rise time on the energy yield of ammonia synthesis are discussed. The inclusion of noble gases expanded the pathway for gas-phase reactions, with the active components of critical reactions examined through optical emission spectra. This analysis revealed an increased presence of both  $N_2^+$  and  $N_2^*$  particles in the reaction's rate-limiting step, attributed to the addition of noble gases. Finally, a zero-dimensional (0D) plasma chemical kinetic model was established to investigate the influence of Ar addition on the reaction mechanism of ammonia synthesis.



**Citation:** Xu, Y.; Yuan, H.; Wang, H.; Lu, K.; Yang, D. Effectiveness of Noble Gas Addition for Plasma Synthesis of Ammonia in a Dielectric Barrier Discharge Reactor. *Appl. Sci.* **2024**, *14*, 3001. <https://doi.org/10.3390/app14073001>

Academic Editor: Francis Verpoort

Received: 7 March 2024

Revised: 24 March 2024

Accepted: 30 March 2024

Published: 3 April 2024



**Copyright:** © 2024 by the authors. Licensee MDPI, Basel, Switzerland. This article is an open access article distributed under the terms and conditions of the Creative Commons Attribution (CC BY) license (<https://creativecommons.org/licenses/by/4.0/>).

**Keywords:** ammonia synthesis; dielectric barrier discharge; non-thermal plasma; optical emission spectra; kinetic modelling

## 1. Introduction

Ammonia is a promising energy source and industrial raw material. In recent years, ammonia has attracted widespread attention [1]. As a carbon-free hydrogen energy carrier, ammonia has the advantage of being safe and easy to store and transport [2]. Ammonia is also of great economic importance as a basic precursor for many essential chemicals [3]. The Haber-Bosch (H-B) process using an iron-based catalyst is the current method of industrial ammonia synthesis. This reaction requires high temperatures (500 °C) and high pressures (200 bar) to proceed [4]. However, the H-B process is responsible for consuming 1–2% of the world's total energy and contributes to 1.6% of global CO<sub>2</sub> emissions [5]. Over the past decades, high temperature and pressure reaction conditions have prevented significant increases in the efficiency of the H-B process, and improvements in catalysts have not resulted in significant increases in energy yields or improvements in economics [6].

In the past few years, many researchers have investigated green, environmentally friendly, and gentle methods for ammonia synthesis. Among them, non-thermal plasma (NTP) technology is a novel solution, especially when combined with catalysts [7]. In the plasma region, collisions between electrons and gas molecules cause various reactions. As a result, low activation barriers are produced under mild reaction conditions, effectively

activating molecules with strong bonds such as  $\text{N}\equiv\text{N}$  triple bonds [7]. The plasma can be initiated and halted at any moment and is flexible to intermittent renewable energy sources, including solar, wind, and hydropower [8]. Plasma ammonia synthesis reaction units are very small and can be adapted to practical conditions for decentralized, small-scale ammonia production. Based on these advantages, plasma-catalyzed ammonia synthesis has great application potential.

To date, researchers have investigated NTP-assisted ammonia synthesis using various types of discharges, including glow discharges [9,10], radio frequency discharges (RF) [11,12] and microwave discharges [13,14], arc discharges [15–17], and dielectric barrier discharges (DBD) [18–20]. Uyama et al. attempted the synthesis of ammonia by NTP using microwave discharges and RF plasma. These processes were performed at a pressure of about 650 Pa, well below atmospheric pressure [21]. However, to eliminate the need for a vacuum and allow for the continuous operation of the system, studies published in recent years have focused on ammonia synthesis using DBD. Gomez et al. described a ferroelectric packed-bed DBD reactor. Two planar electrodes and a filled catalyst form the main body of this reactor. In this study, the ferroelectric material acts as both the catalyst and the electrode [22]. However, in their most recent study using this DBD device coupled with a metal catalyst, although the discharge characteristics could be modified to produce a stronger plasma, ammonia decomposition or hydrogen exchange processes were promoted in the process, and the ammonia synthesis of this reactor was not significantly enhanced [23]. This structure of the DBD makes it easier to couple the plasma to the catalyst to support ammonia synthesis, and improves ammonia synthesis by changing the discharge characteristics of the plasma and adding new chemical kinetic reactions [24]. In addition to the addition of suitable catalysts, the addition of noble gases to gas-phase reactions can also improve plasma utilization. It has been discovered that the addition of noble gases alters the properties of the plasma, which accelerates the chemical reactions within it. Adding noble gases to the RF plasma resulted in much improved ammonia synthesis by Yaala et al. [25]. The addition of Ar to the DBD plasma by Liu et al. resulted in an increase in the conversion of  $\text{N}_2$  of 4.53–8.13%, indicating that the addition of Ar favors the generation of  $\text{NH}_3$  [26]. Patil et al. used a packed-bed DBD plasma to synthesize ammonia by adding a small amount of Ar to the gas feed, which resulted in a 2% increase in ammonia concentration and energy yield, but the addition of excess Ar reduced ammonia production by 5.6% [27]. Zhou et al. modified the plasma characteristics and increased ammonia production by adding He to various configurations of DBD reactors [28]. For different types of plasma, the addition of noble gases under different conditions produces different effects, so it is crucial to study the optimal reaction conditions and synthesis mechanism for the interaction between the reactor and the plasma. From previous work, it can be seen that DBD ammonia synthesis is mostly plasma generated by AC power sources and nanosecond power sources are rarely used for ammonia synthesis. Optimizing the plasma source is one way to improve the use of energy in the process. Nanosecond pulses enable controlled discharges on shorter time scales than AC power sources, allowing electrons to gain high energy in the free range, avoiding energy loss in the gas heating process and providing high efficiency in terms of energy consumption and energy yield. Second, nanosecond pulsed power supplies have more adjustable parameters for better control of plasma properties [29].

In this work, we integrated a nanosecond pulsed power supply with a DBD system to enhance ammonia synthesis by incorporating noble gases, specifically Ar and He. This study thoroughly explored how various gas conditions, noble gas additions, and pulse parameters influenced the rate of ammonia synthesis and its energy yield. Additionally, the impacts of Ar and He additions on plasma characteristics were examined using electrical characterization diagnostics. The analysis of the influence of noble gases on the ammonia synthesis mechanism was conducted using optical emission spectra (OES) and 0D plasma chemical kinetic modeling.

## 2. Experimental Setup and Methods

### 2.1. Experimental Setup

Figure 1 shows a schematic diagram of NTP-assisted ammonia synthesis. The reactor is a coaxial DBD. Stainless steel rods are used as high voltage electrodes. A pulsed power supply (HVP20P, Xi'an Smart Maple Electronic Technology Co., Xi'an, China) capable of delivering voltages up to 30 kV and operating in the frequency range of 100–3000 Hz was used for the experiments. An 80 mm long copper mesh served as the grounding electrode, while a stainless-steel electrode with a 6 mm diameter acted as the high voltage counterpart. The quartz tube featured a 1 mm wall thickness and the gap for discharge was set at 2 mm. Hydrogen was obtained from a hydrogen generator (TH-300, Beijing Institute of Cogeneration Analysis Technology, Beijing, China). A gas mixture of nitrogen (99.999%), hydrogen (99.99%), and argon (99.999%) or helium (99.999%) was introduced into the reactor. Its flow rate and volume ratio were adjusted by a mass flow controller. To capture the electrical characteristics of the plasma within the reactor, an oscilloscope (TDS 3054B, Tektronix Inc., Beaverton, OR, USA) equipped with a current monitor (TCP312A, Tektronix Inc., USA), a voltage probe (P6015A, Tektronix Inc., USA) all supplied by Tektronix, was utilized. OES were recorded and transferred to a grating monochromator (ANDOR SR-750I, Andor Technology, Belfast, UK), and the optical signals were converted to digital models by a CCD (Newton 920, Andor Technology, UK).

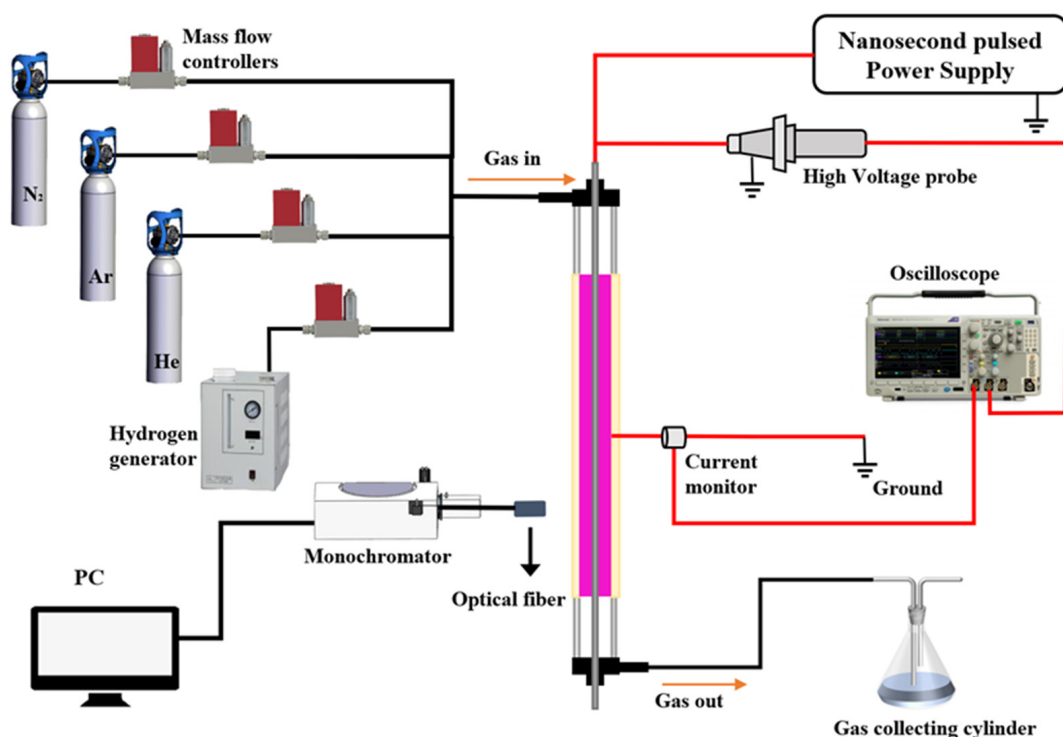


**Figure 1.** Experimental setup for ammonia synthesis by DBD.

### 2.2. Parameters Calculation and Kinetic Model

After the reaction, the tail gas was transferred to 10 mL of 0.005 mol/L H<sub>2</sub>SO<sub>4</sub> dilute, and 0.5 mL of absorbed H<sub>2</sub>SO<sub>4</sub> dilute was transferred to the ammonium nitrogen detector to determine the ammonium concentration. The chemical formula of the reaction is shown in Equation (1):



The measured ammonium concentration was the ammonia concentration. From Equation (2), the ammonia synthesis rate could be calculated as follows:

$$\text{NH}_3 \text{ synthesis rate } (\mu\text{mol} \cdot \text{g}^{-1} \cdot \text{h}^{-1}) = \frac{C(\text{mg} \cdot \text{L}^{-1}) \times 10(\text{mL}) \times 60(\text{min} \cdot \text{h}^{-1})}{18(\text{g} \cdot \text{mol}^{-1}) \times t(\text{min})} \quad (2)$$

where  $C$  is the  $\text{NH}_3$  concentration.  $t$  is reaction time. Equation (3) was used to determine the energy yield ( $\text{g kWh}^{-1}$ ):

$$E_{\text{NH}_3} (\text{g} \cdot \text{kWh}^{-1}) = \frac{\frac{C(\text{mg} \cdot \text{L}^{-1}) \times 10(\text{mL})}{t(\text{min})} \times 60(\text{min} \cdot \text{h}^{-1})}{P(\text{W})} \times 10^{-3} \quad (3)$$

$$P = f \int V(t) \times I(t) dt \quad (4)$$

In Equation (4), " $V(t)$ " is the voltage in "V", " $I(t)$ " is the current in "A", " $f$ " is the frequency in  $\text{s}^{-1}$ .

The experimentally measured spectra of  $\text{N}_2$  ( $\text{C}^3\Pi_u \rightarrow \text{B}^3\Pi_g$ ) were imported into the Specair software (Version 3.0), and the OES curves were fitted to them by setting the parameters of spectral species and the narrow peak coefficient, and adjusting the set values of rotation and vibration temperatures to derive the rotation and vibration temperatures of the nitrogen molecules under the experimental conditions. Given the minimal energy gap between rotational energy levels, the plasma's gas temperature can be closely estimated by the rotational temperature of  $\text{N}_2$ .

A 0D plasma chemistry model was used to understand the key intermediates and chemical pathways following the addition of noble gases. The electron temperature in a non-equilibrium plasma is much higher than the gas temperature, and the electron energy distribution function deviates from the Maxwell distribution, which is subject to the Boltzmann equations, which are too complicated to solve because they include all possible transport and collision terms. The BOLSIG+ Boltzmann equation solver, developed by Hagelaar et al. [30], provided a swift method to approximate the solution of the Boltzmann equation. It utilized two approximations to calculate the electron energy distribution function,  $F_0$ . After the Boltzmann equation was solved and  $F_0$  determined, the rate coefficients for every substance involved in the electron collision reaction process were calculated using Equation (5).

$$k_{je} = v \int_0^\infty \varepsilon \sigma F_0 d\varepsilon \quad (5)$$

In Equation (5),  $k_{je}$  is the electron collision reaction rate coefficient in " $\text{m}^3/\text{s}$ ";  $v$  is the viscosity coefficient in " $\text{Pa} \cdot \text{s}$ ",  $\varepsilon$  is the electron energy in " $\text{eV}$ ";  $\sigma$  is the electron collision cross section, and  $F_0$  is the obtained electron energy distribution function.

When simulating the discharge process, the ZDPlaskin Fortran90 program calls the BOLSIG+ solver to solve the electron transport coefficients and the reaction rate coefficients quickly and in real time, and calls the DVODE\_90 solver to solve the component concentration equations to obtain the reaction rate and the evolution of reactive particles over time during the discharge process.

The support material lists the 51 particles (Table S2), the chemical reactions involved, and the corresponding reaction rate constants (Table S3) considered in the chemical modeling of the synthesis of ammonia with the addition of Ar in nanosecond pulse discharge plasmas.

### 3. Results and Discussion

#### 3.1. Effect of Ar and He Addition on Electrical Characteristics

We compared the discharges without noble gas addition, with Ar addition, and with He addition under the same discharge conditions, with the pulse voltage set to 13 kV, the

pulse repetition frequency set to 1200 Hz, and the amount of noble gas added to 40% of the total gas volume. Maintaining the gas ratio of  $H_2:N_2 = 3$ , the total gas flow rate was set at 120 mL/min without the addition of noble gas, and at 200 mL/min when noble gas was added. Refer to Table S1 for the various gas flow rate configurations (the impact of gas flow rate will be examined subsequently). Figure 2 shows the voltage–current profiles for the three cases of no noble gas addition, Ar addition, and He addition. The figure illustrates that the current's amplitude escalates with the incorporation of Ar and He. Without any noble gas, the current amplitude stands at 18.49 A, but this figure climbs to 25.18 A with Ar and further to 27.24 A with He. This rise in current amplitude is attributed to the reduction in breakdown voltage caused by the addition of Ar and He [26]. The lower breakdown voltage is responsible for its stable discharge at lower energy input [28]. In contrast to the case without noble gas addition, the waveform of the discharge current becomes smoother in the discharge, indicating that the uniformity of the discharge is improved. Previous research has shown that the most significant impact of adding noble gases to discharge plasma is the facilitation of a more uniform and diffuse plasma generation [31]. This is due to the fact that the metastable energy levels of Ar and He atoms are higher in energy than the metastable energy levels of N atoms. The addition of a noble gas to the feed gas results in a Penning reaction, which causes the ionization coefficient to increase, thereby reducing filamentary discharges and making the plasma more uniform and diffuse [32]. In addition, the increase in voltage amplitude is greater for the case of adding He, which also indicates that the discharged power is higher for the case of adding He. This is related to the thermal conductivity of Ar and He. The thermal conductivity of Ar is 0.018 W/mK, compared to He is 0.15 W/mK. The superior thermal conductivity of He contributes to maintaining discharge stability by facilitating rapid heat transfer. In addition, rapid diffusion during discharge contributes to the uniformity and diffusion of the discharge because the diffusion coefficient of He is much higher than that of Ar [28].

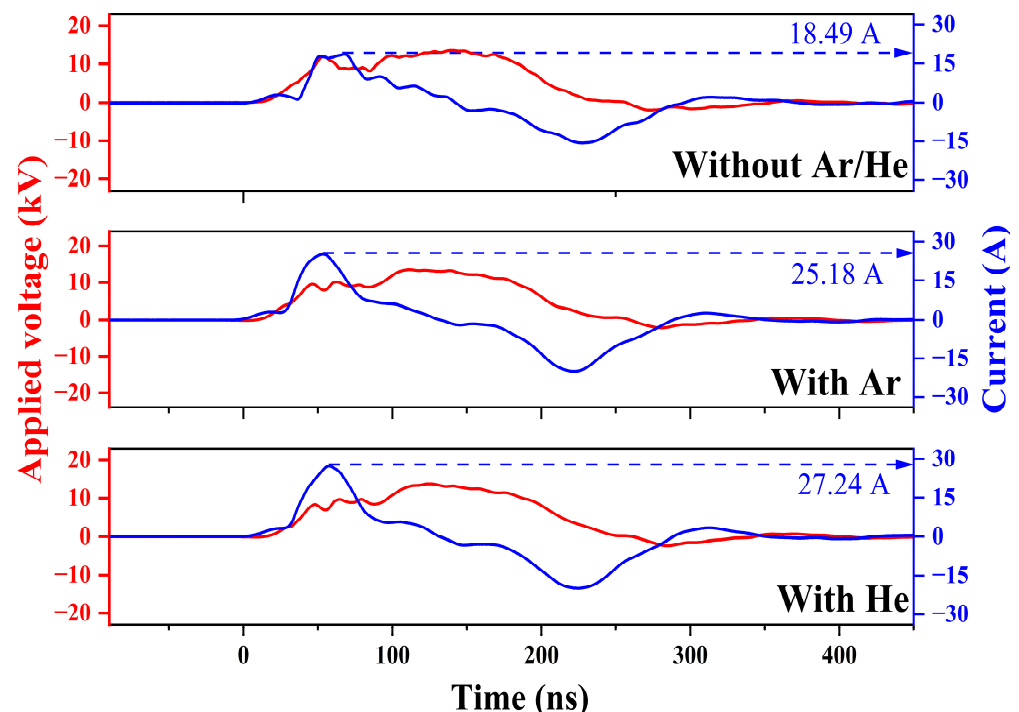


**Figure 2.** Effect of Ar and He addition on voltage–current profile.

### 3.2. Effect of Ar and He Addition on $NH_3$ Formation

In NTP-assisted ammonia synthesis applications, the gas flow rate can affect the ammonia synthesis. The effect of the total gas flow rate on ammonia synthesis was explored using 13 kV, 1200 Hz pulse parameters without noble gas addition, always keeping the gas

ratio  $H_2:N_2 = 3$ . Figure S1 illustrates that elevating the low flow rate enhances both the ammonia synthesis rate and the energy yield. This enhancement plateaus once the flow rate hits 120 mL/min and starts to decline when exceeding 280 mL/min. Increasing the gas flow rate will provide a larger supply of raw reactant gas, thereby increasing the collision probability between reactive particles. This will be beneficial for ammonia production [26]. At the same time, with the shortening of the residence time, the possibility of effective collisions of electrons with the reacting material, both on the surface of the packing and in the gas phase, decreases, thus reducing the rate of  $NH_3$  synthesis [33]. Similarly, Wang et al. combined experiments and calculations to conclude that a reasonable increase in the flow rate would improve the synthesis rate of  $NH_3$ . However, too high a flow rate leads to a decrease in the specific energy input (SEI), which is the main reason for the decrease in  $NH_3$  yield [34]. Based on the experimental results, we conclude that increasing the initial number of reactants significantly increases the efficiency of ammonia synthesis at low flow rates. Once the “synthesis capacity” of the system is reached, the reduction in the SEI and the shortened reaction time result in a decrease in the rate of ammonia synthesis. In the experiments investigating the effect of noble gas addition on ammonia synthesis, the total gas flow rate was always maintained at 120–280 mL/min. Although the ammonia synthesis rate and energy yield decreased slightly in this flow rate range, the ammonia synthesis rate did not decrease by more than 5.76% and the energy yield did not decrease by more than 8.06%. Therefore, it was considered to be a stable “flow rate window”. The flow rates of the added gases under various conditions are shown in Table S1.

Under the same pulse parameters (13 kV, 1200 Hz), the effect of the feed gas ratio and adding noble gases to different feed gas ratios on the effect of ammonia synthesis was investigated. Figure 3 shows the energy yield of ammonia synthesis with different raw gas ratios and with the addition of Ar and He to different raw gas ratios. As shown in the figure, the energy yield of ammonia synthesis without the addition of Ar and He increases with the nitrogen content and has a maximum value of 0.417 g- $NH_3$ /kWh at  $H_2:N_2 = 3$ . Beyond this ratio, the energy yield starts to decrease with increasing nitrogen content. This is consistent with the gas ratios in the theoretical reaction ( $N_2 + 3H_2 \leftrightarrow 2NH_3$ ) [35]. The dissociation of  $N \equiv N$  is the rate-limiting step of the entire reaction, owing to the significantly higher dissociation energy of  $N_2$  (9.75 eV) compared to that of  $H_2$  (4.52 eV) [36]. When the value of  $H_2:N_2$  changes from 3 to 5, the energy yield decreases, which suggests that increasing the  $H_2$  content also decreases the energy utilization because excess active hydrogen contributes to ammonia decomposition. Energy yield also begins to decrease when the  $H_2:N_2$  ratio exceeds 3. Increasing the  $N_2$  concentration beyond the optimum ratio will use less  $H_2$  for ammonia production. With the addition of noble gases, the optimal ratio of gases changed; the optimal ratio with the addition of Ar was  $H_2:N_2 = 1$ , while the optimal ratio with the addition of He was  $H_2:N_2 = 2$ . The different optimal ratios observed with no noble gas addition and with different noble gas additions are due to the different sensitivities of the optimal gas ratios to the reduced field in the reaction and to the electron density in the reactor [37]. The addition of either Ar or He increased the energetic yield of  $NH_3$  synthesis in all gas ratios. The introduction of noble gas improved the discharge conditions and increased the electron density in the reactor, which had a positive effect on ammonia synthesis [38]. Furthermore, additional non-surface reactions (described in detail in a later section) promoting ammonia synthesis will be provided by new collisional particles such as  $Ar^*$ ,  $He^*$ , etc.

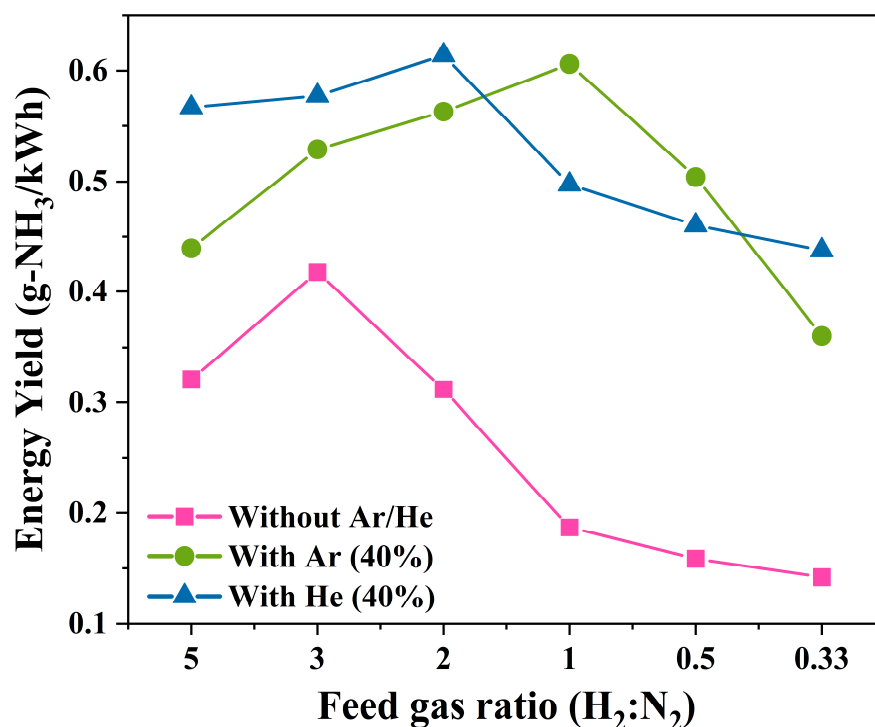


**Figure 3.** Effect on ammonia synthesis energy yield of adding noble gases at different feed gas ratios.

To study the effect of the amount of noble gas added on the synthesis of ammonia, we added different amounts of noble gas at different feed gas ratios. Figure 4a,b illustrate how different additions of Ar and He at different gas ratios affect the energy yield in ammonia synthesis. According to the data presented, optimal results were obtained with both Ar and He additions at a ratio of 40%. Beyond this point, the energy yield of ammonia synthesis begins to decrease as the additions increase. The diminished lifting effect observed at a gas ratio of H<sub>2</sub>:N<sub>2</sub> = 3 stems from the shift in the optimal gas ratio caused by the incorporation of noble gases. This result indicates that moderate addition of noble gases is favorable for ammonia synthesis, while excessive addition of noble gases can have a negative effect on ammonia synthesis. In the previous analysis, we concluded that the addition of an appropriate amount of noble gas can optimize discharge uniformity, while the addition of noble gas adds more collision particles to the reaction, increasing the likelihood of inelastic collisions and thus increasing the production of intermediate reaction products. However, in the case of further ionization, the increase in metastable Ar\* and He\* helps to maintain the plasma for a longer period of time, a process that may promote ammonia decomposition [28,39]. In a later section, we will discuss the fact that the number of active particles in the metastable state increases with the addition of noble gases. When the density of the reacting species reaches its optimum level, further addition of noble gas changes the properties of the plasma, leading to an increase in both electron density and electron energy. This enhancement triggers additional decomposition of the intermediate product NH<sub>x</sub> in the gas phase [31]. Additionally, More energy is wasted on ionization and excitation of Ar and He than the dissociation of N<sub>2</sub> and H<sub>2</sub> when noble gases are added at too high a concentration [40].

Figure 4 demonstrates that the energy yield from ammonia synthesis notably improves as the nitrogen content increases, whereas the optimal gas ratio remains unchanged with an increase in noble gas content. The addition of noble gases increases the average electron energy and electron density, making N<sub>2</sub> easier to dissociate. For a given energy input, the conversion of N<sub>2</sub> increases with the addition of Ar and He, thus shifting the optimum gas ratio to a higher nitrogen concentration by noble gas injection. Figure S2 illustrates that the discharge power escalates with an augmentation in N<sub>2</sub> content, aligning with the findings

of Brand et al., who reported that incorporating Ar into the gas mix enhances the average electric field strength [41]. It should be noted that too much H<sub>2</sub> leads to a weakening of the ammonia synthesis. The increase in metastable H\* in the plasma undergoes a quenching reaction, and the intensity of the plasma discharge weakens as the H<sub>2</sub> content increases [42].

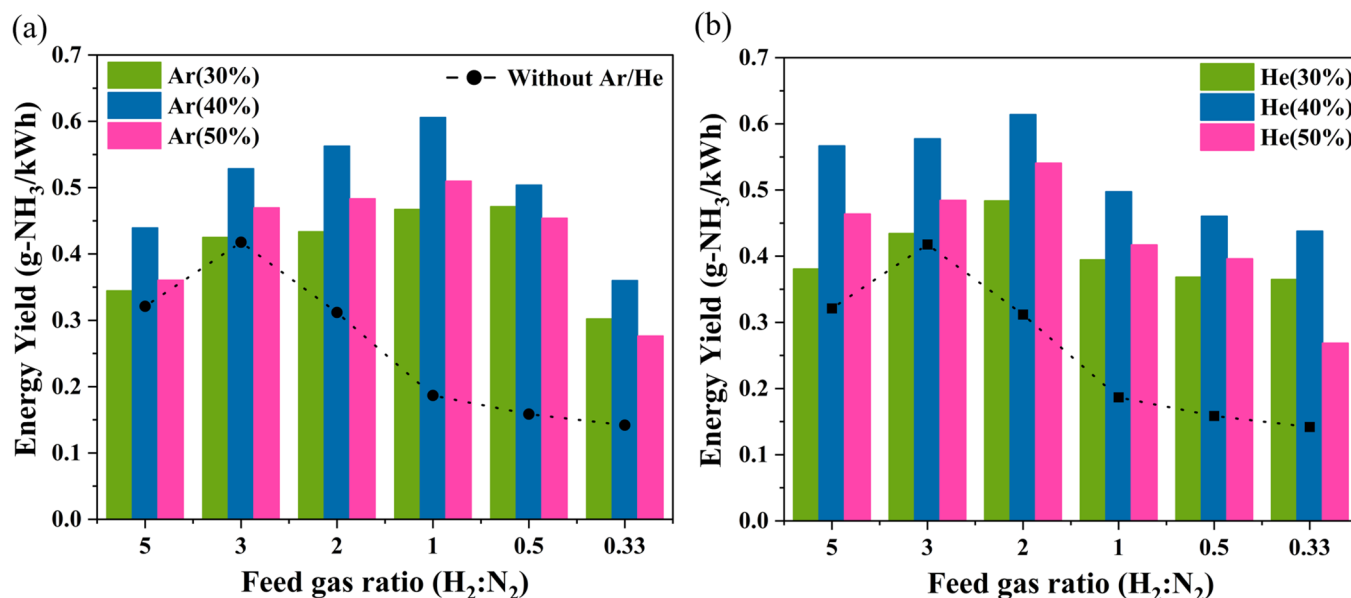


**Figure 4.** Effect of the addition of (a) Ar and (b) He on the energy yield of the synthesis of ammonia.

### 3.3. Effect of Discharge Parameters on NH<sub>3</sub> Formation

The impact of pulse voltage on the discharge is notably crucial, given that pulse voltage is instrumental in the ionization process of N<sub>2</sub> and H<sub>2</sub>. Figure 5a,b show the effect of different pulse voltages on the effect of ammonia synthesis. As shown in Figure 5a, without addition of noble gases, the ammonia synthesis rate rises and then decreases with increasing voltage, indicating that when the voltage exceeds 13 kV, more input energy can promote the ammonia decomposition reaction. After the addition of noble gas, the ammonia synthesis rate did not decrease with increasing voltage. The increase of voltage makes the ionization of gas molecules more intense, which makes the rate of electron collision reaction greatly increase, so the increase in voltage can effectively promote ammonia synthesis. Figure 5b shows that after introducing Ar and He, the ammonia synthesis rate rises with an increase in voltage, yet the peak energy yield for both is attained at 13 kV. This means that after the discharge voltage exceeds 13 kV, the energy utilization of ammonia synthesis decreases with increasing voltage for the same input energy. Since the increase in voltage also increases the probability that Ar and He will collide with electrons, this consumes some of the input energy. As for the increase in the rate of ammonia synthesis, we attribute it to the increase in the number of active particles of Ar and He, whose collisions with other particles produce more reactive substances such as N<sub>2</sub><sup>+</sup>, N<sub>2</sub><sup>\*</sup>, and H<sub>2</sub><sup>\*</sup>. The mechanism of generation of active species will be described in detail later. This is because more non-surface reaction pathways compared to the case without the addition of noble gases means that intermediate reactants can be produced by more particle collisions, especially reactive particles of N<sub>2</sub>, which have the rate-limiting effect on the reaction [43].

Figure 5c,d illustrate how variations in pulse frequency impact the rate of ammonia synthesis and the efficiency of energy yield. Increasing the pulse repetition frequency increases the electron density and the amount of active material due to the increased energy input within the discharge period. Figure 5c reveals that the rate of ammonia synthesis progressively rises with an increase in pulse repetition frequency. The reason is that a higher pulse frequency augments the charge within the discharge channel, thereby enhancing discharge activity. This amplification in discharge intensity boosts collision

chances, leading to a surge in high-energy electron generation per unit time, which in turn elevates the ammonia synthesis rate. Figure 5d shows that the energy yields for both the cases without and with the addition of noble gases have a maximum at a pulse repetition frequency of 1200 Hz. The pulse repetition frequency begins to decrease when it exceeds 1200 Hz, and too high a pulse repetition frequency leads to a decrease in energy yield. The power formula indicates that a rise in frequency corresponds to an increase in discharge power. However, the energy yield from ammonia synthesis diminishes when the pulse repetition frequency becomes excessively high. However, for ammonia synthesis, which is a reversible reaction, we cannot intuitively determine from the conclusions whether an increase in frequency results in facilitated ammonia decomposition.

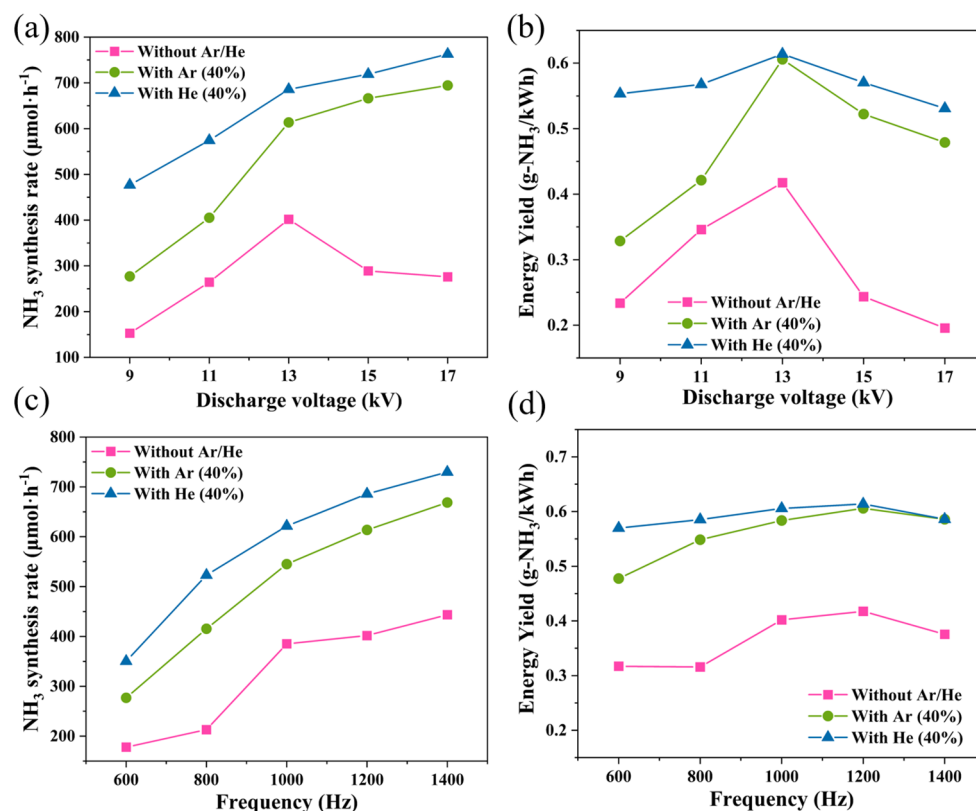


**Figure 5.** Effects of pulse voltage and pulse repetition frequency on (a,c) the rate of ammonia synthesis and (b,d) the energy yield.

The effect of pulse width on the rate and energy yield in the three systems is shown in Figure 6a,b. It can be seen that increasing the pulse width decreases the energy yield. Increasing the pulse width decreased both the synthesis rate and the energy yield without the addition of noble gases. In contrast, the addition of Ar and He gave the best results at a pulse width of 120 ns. As the pulse width increases from 100 ns to 120 ns, the energy input and discharge time also increase, and the number of high-energy electrons and reactive species involved in the ammonia synthesis reaction increases, which facilitates the promotion of ammonia synthesis. The essence of the pulse width is the discharge time of the highest voltage of a single pulse of a nanosecond pulse, in which the prolongation of the discharge time of a single pulse continuously excites the active particles and reduces the relaxation process of the active groups [44]. Increasing pulse width in plasma-assisted ammonia synthesis experiments can raise energy input, but extending the single-pulse maximum voltage discharge time beyond the optimal pulse width can negatively affect ammonia synthesis, promoting its decomposition. Comparing pulse voltage and pulse width, increasing pulse voltage boosts energy input without extending relaxation time, while increasing pulse width maintains energy input per unit time, prolonging pulse

duration. Due to plasma's unique properties, reactions occur on very short timescales; extending discharge time can decompose produced ammonia, reducing energy yield [29]. Appropriately increasing pulse width injects more energy into the reaction, but exceeding optimal parameters leads to the decomposition of synthesized ammonia; the optimal pulse width parameter is a balance between energy input and efficient utilization of the input energy. Thus, controlling energy input over time is crucial for studying the impact of pulse width on ammonia synthesis. Notably, gas breakdown characteristics vary with pulse width, with shorter pulses (1 ns) breaking down after the pulse and longer pulses (100 ns) during the pulse, highlighting pulse width's influence on plasma properties [45].

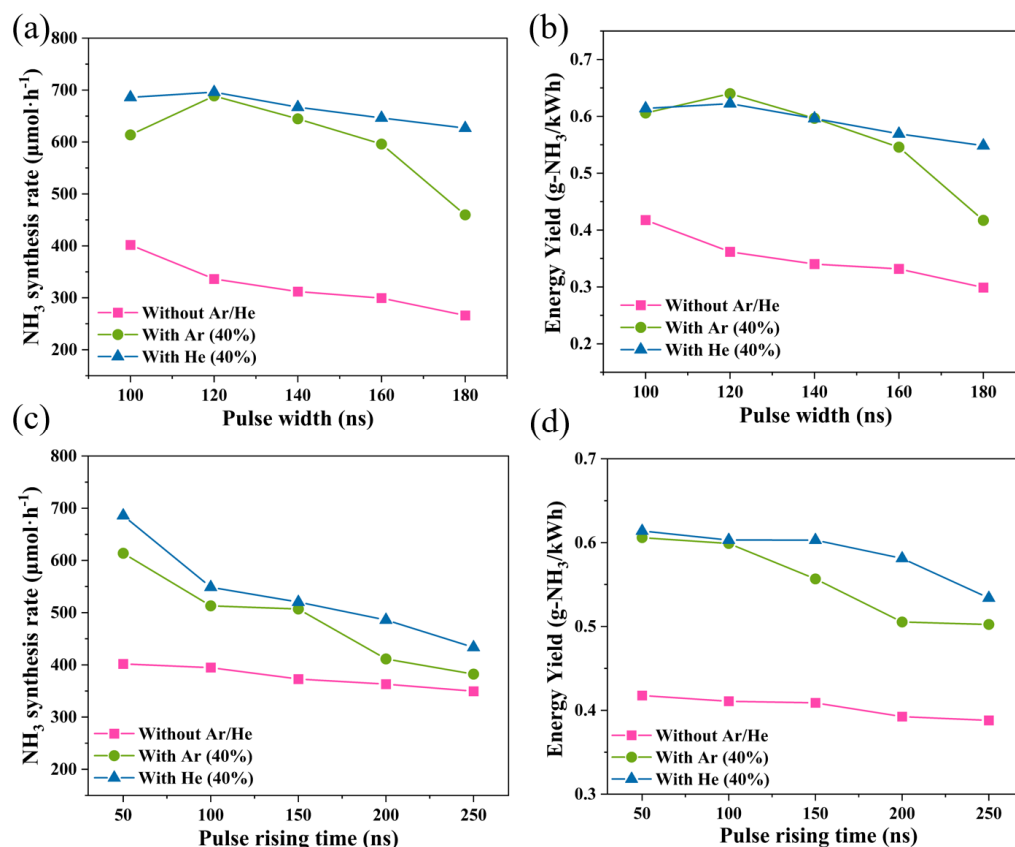


**Figure 6.** Effect of pulse width on (a) the rate of ammonia synthesis and (b) the energy yield and effect of pulse rising time on (c) the rate of ammonia synthesis and (d) the energy yield.

During operation of a pulsed power supply, the time it takes for the voltage to rise from zero to the maximum voltage is known as the pulse rise time. The excited state particles produced in the plasma have short lifetimes. The pulse rise time directly determines the properties of the plasma [46]. Figure 6c,d depict how varying pulse rise times impact the rate of ammonia synthesis and the efficiency of energy yield. As depicted in the figure, both the rate of ammonia synthesis and the energy yield diminish as the pulse rise time increases, with a more pronounced effect observed in the presence of noble gas addition. A shorter pulse rise time means a faster change in voltage over time, which favors the generation of a higher reduced field, thus increasing the average electron energy, leading to an increase in the probability of excitation or dissociation of N<sub>2</sub> and H<sub>2</sub> [47]. Similarly, increasing the pulse rise time results in a longer reaction time during which the NH<sub>3</sub> produced has a higher probability of colliding with electrons or other particles, leading to decomposition.

### 3.4. OES of Plasma with Addition of Ar and He

The intensities of the characteristic spectral lines represent the relative concentrations of the corresponding species, and Figure S3 presents the OES for the cases of adding Ar

and He, highlighting the characteristic peaks at specific wavelengths. Figure 7 shows the OES of the  $N_2$  second positive system ( $N_2$  ( $C^3\Pi_u \rightarrow B^3\Pi_g$ , 337.1 nm)) and the  $N_2^+$  first negative system ( $N_2^+$  ( $B^2\Sigma_u^+ \rightarrow X^2\Sigma_g^+$ , 391.4 nm)) for Ar and He, respectively. This suggests that electronic excitation (6) and ionization (7) reactions occur during the synthesis of ammonia. As can be seen in Figure 7, the intensities of the  $N_2^*$  and  $N_2^+$  spectral lines increase with increasing Ar and He content, a phenomenon that suggests that electronic excitation and ionization reactions occur more strongly with increasing noble gas addition. Combined with experimental results, increasing the number of reactive particles in the gas phase reaction improves ammonia synthesis, but OES was unable to quantify whether the reactive particles were more involved in the forward or reverse reaction. However, despite the higher strength of  $N_2^*$  and  $N_2^+$  at higher additions of noble gases, the experimental results show that the energy yield of ammonia synthesis with 50% Ar and 50% He is lower than that with 40% Ar and 40% He. Because the energy of metastable He exceeds the ionization energy of  $N_2$ , they generate  $He^+$  particles through charge transfer between  $N_2$  and metastable  $He^*$ . (8), and the  $He_2^+$  particles collide with  $N_2$  to produce  $N_2^+$  (9) at a very high reaction rate [28]. Similarly, the metastable  $Ar^*$  collides with  $N_2$  to form  $N_2^+$  [48]. This collision process is thus facilitated with increasing noble gas additions, which also leads to an increase in the excited state  $N_2^+$  content with increasing noble gas additions.

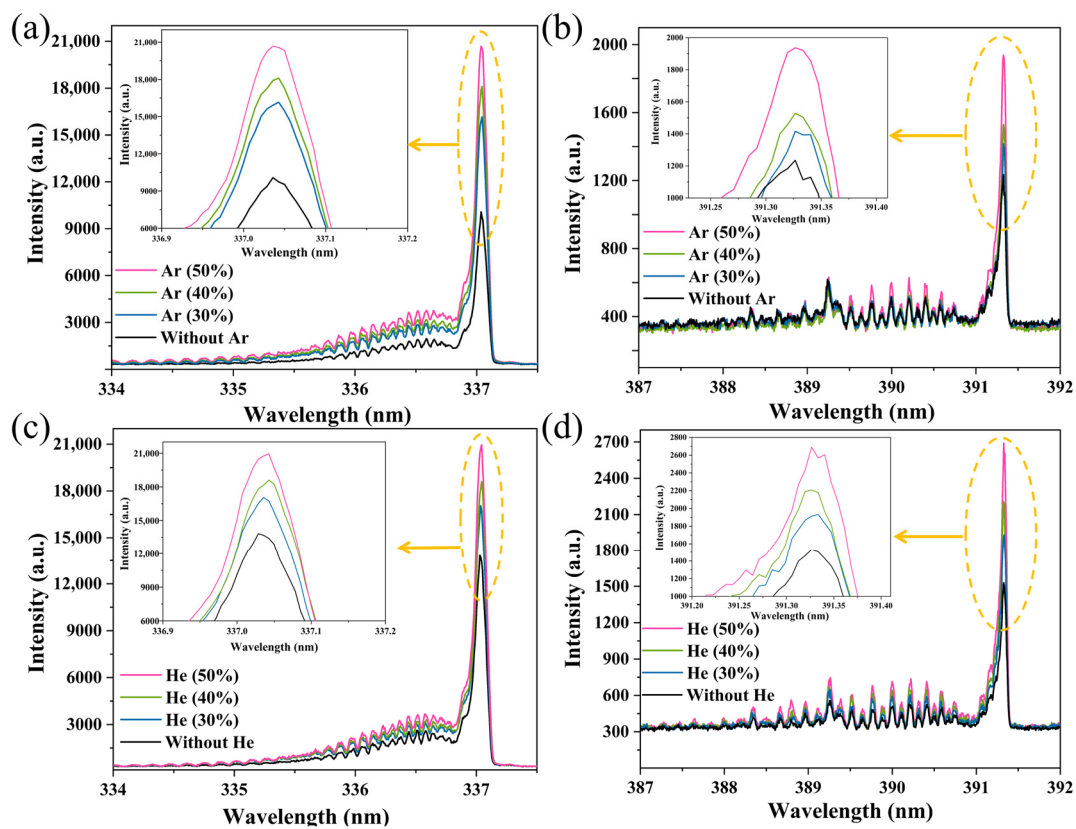
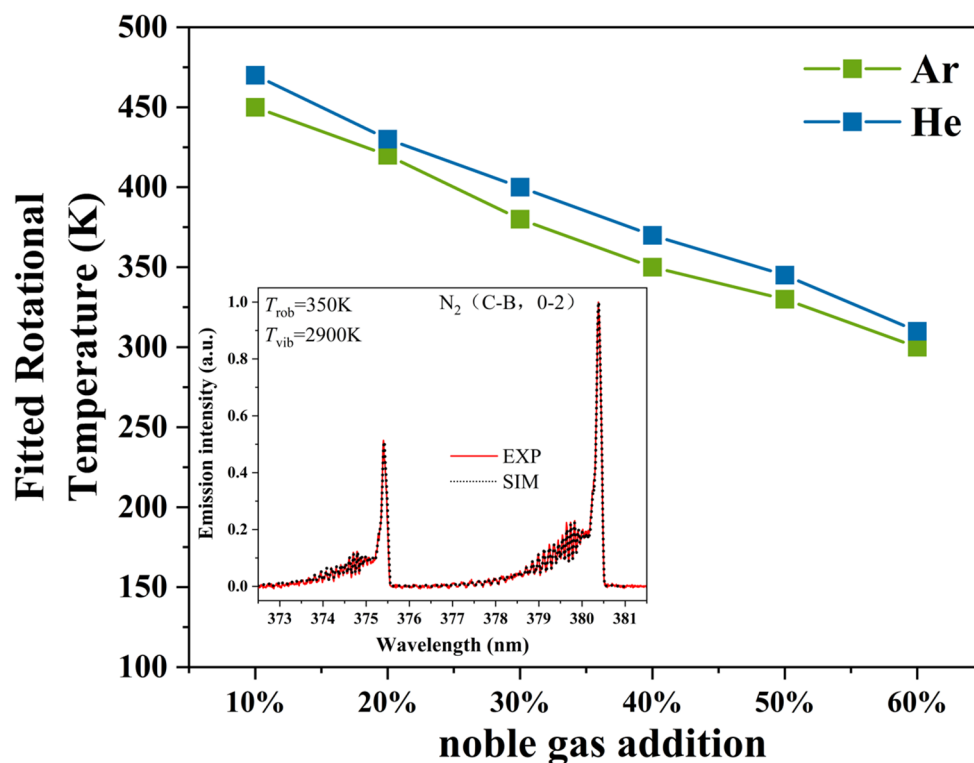


Figure 7. Influence of the content of (a,b) Ar and (c,d) He on the spectra of  $N_2^*$  and  $N_2^+$ .

The properties of the plasma can be significantly altered by the addition of noble gases. We used Specair software to fit the OES of  $N_2^+$ (B-X) to derive the gas temperature

under experimental conditions. Electrons gain energy from the electric field and transfer it to other particles through collisions; the vibrational excitation of  $N_2$  helps to lower the dissociation potential barriers to produce more intermediate species [49]. Figure 8 shows the effect of noble gas addition on gas temperature. As can be seen from the figure, the rotational temperature decreases as the amount of noble gas added increases, indicating that more energy is being used to dissociate  $N_2$ . In particular, gas temperature also has an important effect on ammonia synthesis; in previous reports, elevated temperatures promote particle collisions, while excessive temperatures can cause decomposition reactions in the ammonia produced [50].



**Figure 8.** Effect of different Ar and He additions on rotational temperature.

### 3.5. $NH_3$ Generation Mechanism

In order to further investigate the reaction mechanism of ammonia synthesis by pulsed discharge plasma after the addition of noble gases, we analyzed the main reactions after the addition of Ar using a 0D ZDPlaskin reaction kinetics model. In this model, we used the optimal reaction conditions, i.e., the gas ratio of  $N_2:H_2 = 1$ , the addition of Ar of 40%, the pulse voltage of 13 kV, and the pulse repetition frequency of 1200 Hz.

Figure S4 represents the time-dependent changes in the density of the main reactive species during ammonia synthesis by nanosecond pulse plasma. The solid lines in the figures represent the initial reactants  $N_2$ ,  $H_2$ , and the product  $NH_3$ , respectively. In each discharge cycle, the species density shows a periodic pattern. Within a discharge cycle, the number of active particles increases at the onset of discharge due to the energy provided by the discharge, leading to the ionization and dissociation of the initial reactants into intermediate active species. During the intervals between discharges, the active particles and radicals lose external energy, leading to a reduction reaction and a decrease in density. Within a single pulse discharge, there is significant variability in the concentration of different particles. In previous studies, within systems containing only  $N_2$  and  $H_2$ , the density of N typically ranged between  $10^8$  and  $10^{12} \text{ cm}^{-3}$ , and the density of H between  $10^{10}$  and  $10^{16} \text{ cm}^{-3}$ . However, after adding Ar, the density of N ranges between  $10^{10}$  and  $10^{18} \text{ cm}^{-3}$ , and the density of H between  $10^{16}$  and  $10^{19} \text{ cm}^{-3}$  (compared under the same

voltage conditions, as discharge voltage can alter particle density) [51]. This indicates that the involvement of Ar promotes the dissociation of  $N_2$  and  $H_2$ . The lower density of N compared to H also suggests that the dissociation of  $N_2$  is the rate-limiting step in the entire ammonia synthesis reaction. The intermediate species NH and  $NH_2$  are at a lower magnitude, only increasing in particle density at the start of discharge, indicating that the ammonia synthesis reaction primarily occurs with the involvement of discharge plasma.

According to the previous studies,  $N_2^+$ , N, and  $H^*$  were considered as important initial reactants.  $NH_x$  species were also considered as important intermediates [52,53]. By facilitating a charge transfer reaction with  $N_2$  (10), the introduction of Ar augmented the density of  $N_2^+$  ions. A similar charge transfer process is observed between  $Ar^+$  and  $H_2$  (11) [54]. Figure 9 shows the conversion between Ar and  $Ar^+$ . As shown in Figure 9, the decrease in Ar particle density indicates that Ar is consumed throughout the reaction, Ar collides with electrons to produce  $Ar^+$  (12), and the reaction of  $Ar^+$  with  $N_2$  and  $H_2$  increases the particle density of  $N_2^+$  and  $H_2^+$ . At the beginning of the discharge, as the charge transfer between  $Ar^+$  and  $N_2$  and  $H_2$  is reduced to Ar, and the particle density of Ar increases, but is always lower than in the previous discharge cycle.

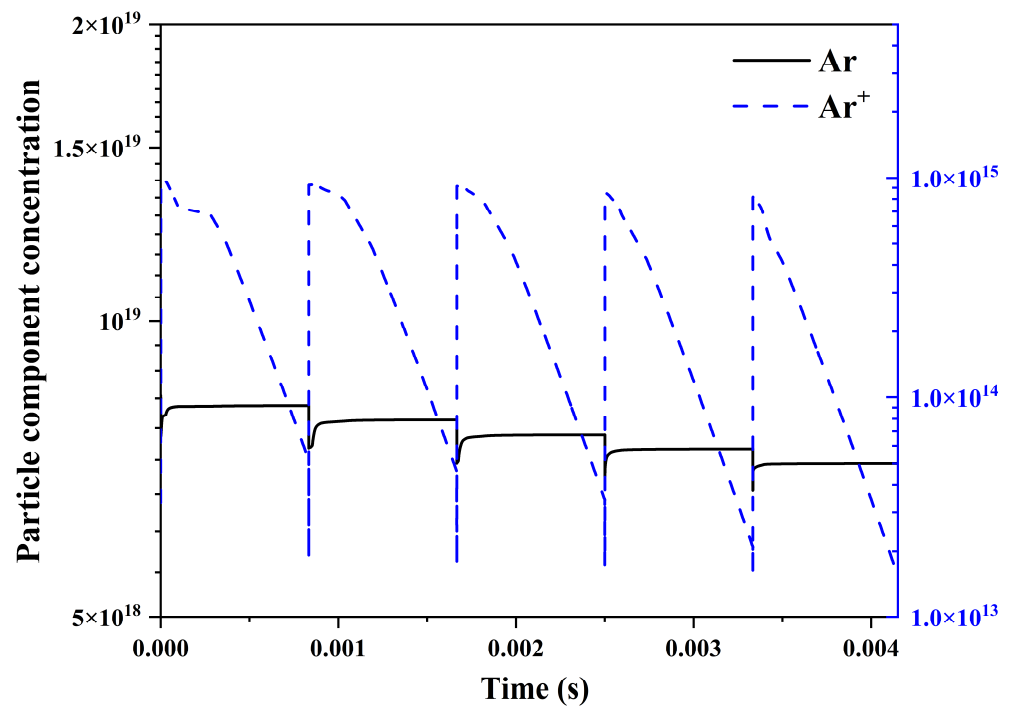


Figure 9. Varying Ar and  $Ar^+$  densities with time in reaction.

The effect of different additions of Ar on the rate of the charge transfer reaction is shown in Figure 10. Adding Ar leads to a higher rate of the charge transfer reaction, suggesting a rise in the likelihood of inelastic collisions. This is indicative of elevated densities of  $N_2^+$  and  $H_2^+$ , a finding that aligns with the OES outcomes presented in Figure 7b. In addition to the enhanced electron collision reaction, the enhancement of the Penning excitation and ionization reactions also leads to enhanced  $N_2$  dissociation. Ar atoms can be excited to form  $Ar^*$  and  $Ar^+$ , and the energy stored in these reactive species can be used in the Penning excitation and ionization reaction, which aids in generating intermediate reactive species, thereby enhancing the synthesis of ammonia [26,55].



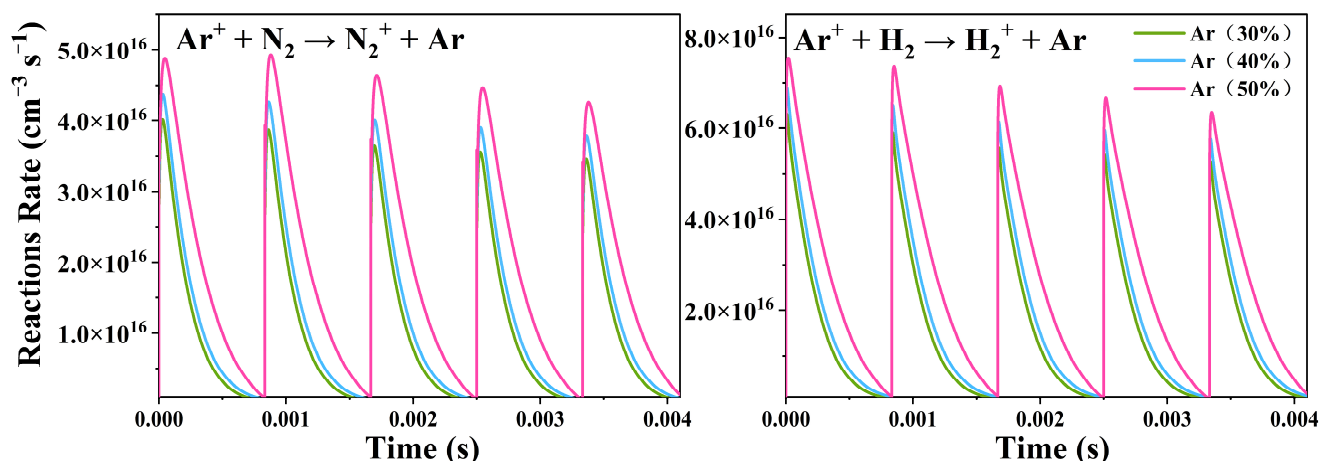


Figure 10. Effect of different additions of Ar on chemical reaction rates.

#### 4. Conclusions

In this work, NTP-assisted ammonia synthesis by the addition of noble gases in a DBD reactor driven with nanosecond pulsed power supply is investigated. The addition of He produces a more uniform and diffuse plasma than the addition of Ar. The addition of noble gases significantly improves the ammonia synthesis effect, and the addition of moderate amounts of noble gases accelerates the production of key reactive particles through penning excitation and ionization reactions. The excessive noble gas additions can lead to ammonia decomposition, as well as more energy wasted on Ar and He excitation and ionization, and reduced energy utilization. By optimizing the reaction conditions, i.e., 40% addition of Ar, gas ratio of  $\text{H}_2:\text{N}_2 = 2$ , 40% addition of He, gas ratio of  $\text{H}_2:\text{N}_2 = 3$ , and the optimum parameters of the pulses, i.e., pulse voltage of 13 kV, pulse repetition rate of 1200 Hz, pulse width of 120 ns, and pulse rise time of 50 ns, the addition of Ar can increase the ammonia synthesis energy yield by 45.1%, and the addition of He can increase it by 47%. The energy yield was increased by 45.1% with the addition of Ar and 47% with the addition of He. We have studied the key reactive particles by OES and found that the number of particles of both  $\text{N}_2^+$  and  $\text{N}_2^*$  in the rate-limiting step of the reaction increases with the addition of noble gases. To further investigate the process, the reaction involving Ar active particles was simulated using the 0D plasma chemical dynamic model. The addition of Ar adds new gas-phase reaction pathways, and as the addition increases, the rate of electron transfer reactions and intermediate reactive species increases, which can facilitate ammonia synthesis.

**Supplementary Materials:** The following supporting information can be downloaded at: <https://www.mdpi.com/article/10.3390/app14073001/s1>. The supplementary materials include settings for gas flow rate parameters, the impact of gas flow rate on ammonia synthesis, the effect of discharge power on ammonia synthesis, additional information on OES, changes in the density of main active species over time, and relevant content involved in modeling. Table S1: Flow rate of additive gases under various conditions. Table S2: Species considered in the  $\text{N}_2\text{-H}_2\text{-Ar}$  plasma model. Table S3: Gas-phase reactions. Figure S1: Effect of Gas Flow Rate on Ammonia Synthesis Efficiency. Figure S2: Effect of different Ar and He additions on the discharge power at different gas ratios. Figure S3: OES plots for the addition of Ar and the addition of He. Figure S4: Variation of the density of the main active particles in the reaction as a function of time.

**Author Contributions:** Methodology and investigation, D.Y. and Y.X.; data curation, and writing—original draft preparation, Y.X.; writing—review and editing, H.Y., H.W. and K.L. All authors have read and agreed to the published version of the manuscript.

**Funding:** This study is supported by the National Natural Science Foundations of China (Grant Nos. 52077026, 12305279 and 52307163), and the China Postdoctoral Science Foundation (2022M710590).

**Data Availability Statement:** Data is contained within the article or supplementary material.

**Conflicts of Interest:** The authors declare no conflicts of interest.

## References

1. Peng, P.; Chen, P.; Schiappacasse, C.; Zhou, N.; Anderson, E.; Chen, D.; Liu, J.; Cheng, Y.; Hatzenbeller, R.; Addy, M.; et al. A Review on the Non-Thermal Plasma-Assisted Ammonia Synthesis Technologies. *J. Clean. Prod.* **2018**, *177*, 597–609. [\[CrossRef\]](#)
2. Zhang, J.; Li, X.; Zheng, J.; Du, M.; Wu, X.; Song, J.; Cheng, C.; Li, T.; Yang, W. Non-Thermal Plasma-Assisted Ammonia Production: A Review. *Energy Convers. Manag.* **2023**, *293*, 117482. [\[CrossRef\]](#)
3. Peng, P.; Schiappacasse, C.; Zhou, N.; Addy, M.; Cheng, Y.; Zhang, Y.; Ding, K.; Wang, Y.; Chen, P.; Ruan, R. Sustainable Non-Thermal Plasma-Assisted Nitrogen Fixation—Synergistic Catalysis. *ChemSusChem* **2019**, *12*, 3702–3712. [\[CrossRef\]](#) [\[PubMed\]](#)
4. Hosseini, H. Dielectric Barrier Discharge Plasma Catalysis as an Alternative Approach for the Synthesis of Ammonia: A Review. *RSC Adv.* **2023**, *13*, 28211–28223. [\[CrossRef\]](#)
5. Zeng, X.; Zhang, S.; Liu, Y.; Hu, X.; Ostrikov, K.K.; Shao, T. Energy-Efficient Pathways for Pulsed-Plasma-Activated Sustainable Ammonia Synthesis. *ACS Sustain. Chem. Eng.* **2023**, *11*, 1110–1120. [\[CrossRef\]](#)
6. Zhou, D.; Zhou, R.; Zhou, R.; Liu, B.; Zhang, T.; Xian, Y.; Cullen, P.J.; Lu, X.; Ostrikov, K. Sustainable Ammonia Production by Non-Thermal Plasmas: Status, Mechanisms, and Opportunities. *Chem. Eng. J.* **2021**, *421*, 129544. [\[CrossRef\]](#)
7. Carreon, M.L. Plasma Catalytic Ammonia Synthesis: State of the Art and Future Directions. *J. Phys. D Appl. Phys.* **2019**, *52*, 483001. [\[CrossRef\]](#)
8. Zeng, X.; Zhang, S.; Hu, X.; Zhang, C.; Ostrikov, K.; Shao, T. Recent Advances in Plasma-Enabled Ammonia Synthesis: State-of-the-Art, Challenges, and Outlook. *Faraday Discuss.* **2023**, *243*, 473–491. [\[CrossRef\]](#)
9. de Castro, A.; Alegre, D.; Tabarés, F.L. Influence of Residence Time and Helium Addition in the Ammonia Formation on Tungsten Walls in N<sub>2</sub>-H<sub>2</sub> Glow Discharge Plasmas. *Nucl. Mater. Energy* **2017**, *12*, 399–404. [\[CrossRef\]](#)
10. Bazinette, R.; Paillol, J.; Massines, F. Optical Emission Spectroscopy of Glow, Townsend-like and Radiofrequency DBDs in an Ar/NH<sub>3</sub> Mixture. *Plasma Sources Sci. Technol.* **2015**, *24*, 055021. [\[CrossRef\]](#)
11. Yaala, M.B.; Saeedi, A.; Scherrer, D.-F.; Moser, L.; Steiner, R.; Zutter, M.; Oberkofler, M.; Temmerman, G.D.; Marot, L.; Meyer, E. Plasma-Assisted Catalytic Formation of Ammonia in N<sub>2</sub>-H<sub>2</sub> Plasma on a Tungsten Surface. *Phys. Chem. Chem. Phys.* **2019**, *21*, 16623–16633. [\[CrossRef\]](#) [\[PubMed\]](#)
12. Shah, J.; Wang, W.; Bogaerts, A.; Carreon, M.L. Ammonia Synthesis by Radio Frequency Plasma Catalysis: Revealing the Underlying Mechanisms. *ACS Appl. Energy Mater.* **2018**, *1*, 4824–4839. [\[CrossRef\]](#)
13. Hu, J.; Wildfire, C.; Stiegman, A.E.; Dagle, R.A.; Shekhawat, D.; Abdelsayed, V.; Bai, X.; Tian, H.; Bogle, M.B.; Hsu, C.; et al. Microwave-Driven Heterogeneous Catalysis for Activation of Dinitrogen to Ammonia under Atmospheric Pressure. *Chem. Eng. J.* **2020**, *397*, 125388. [\[CrossRef\]](#)
14. Bai, X.; Tiwari, S.; Robinson, B.; Killmer, C.; Li, L.; Hu, J. Microwave Catalytic Synthesis of Ammonia from Methane and Nitrogen. *Catal. Sci. Technol.* **2018**, *8*, 6302–6305. [\[CrossRef\]](#)
15. Indumathy, B.; Ananthanarasimhan, J.; Rao, L.; Yugeswaran, S.; Ananthapadmanabhan, P.V. Catalyst-Free Production of Ammonia by Means of Interaction between a Gliding Arc Plasma and Water Surface. *J. Phys. D Appl. Phys.* **2022**, *55*, 395501. [\[CrossRef\]](#)
16. Muzammil, I.; Lee, D.H.; Dinh, D.K.; Kang, H.; Roh, S.A.; Kim, Y.-N.; Choi, S.; Jung, C.; Song, Y.-H. A Novel Energy Efficient Path for Nitrogen Fixation Using a Non-Thermal Arc. *RSC Adv.* **2021**, *11*, 12729–12738. [\[CrossRef\]](#) [\[PubMed\]](#)
17. Zhang, Y.; Liu, B.; Luo, J.; Nie, L.; Xian, Y.; Lu, X. Research on Key Influencing Factors and Mechanisms of Improved Nitrogen Fixation Efficiency in Magnetic-Driven Gliding Arc. *J. Phys. D Appl. Phys.* **2023**, *57*, 125204. [\[CrossRef\]](#)
18. Shah, J.; Wu, T.; Lucero, J.; Carreon, M.A.; Carreon, M.L. Nonthermal Plasma Synthesis of Ammonia over Ni-MOF-74. *ACS Sustain. Chem. Eng.* **2019**, *7*, 377–383. [\[CrossRef\]](#)
19. Zhu, X.; Hu, X.; Wu, X.; Cai, Y.; Zhang, H.; Tu, X. Ammonia Synthesis over  $\gamma$ -Al<sub>2</sub>O<sub>3</sub> Pellets in a Packed-Bed Dielectric Barrier Discharge Reactor. *J. Phys. D Appl. Phys.* **2020**, *53*, 164002. [\[CrossRef\]](#)
20. van 't Veer, K.; Engelmann, Y.; Reniers, F.; Bogaerts, A. Plasma-Catalytic Ammonia Synthesis in a DBD Plasma: Role of Microdischarges and Their Afterglows. *J. Phys. Chem. C* **2020**, *124*, 22871–22883. [\[CrossRef\]](#)
21. Uyama, H.; Nakamura, T.; Tanaka, S.; Matsumoto, O. Catalytic Effect of Iron Wires on the Syntheses of Ammonia and Hydrazine in a Radio-Frequency Discharge. *Plasma Chem. Plasma Process.* **1993**, *13*, 117–131. [\[CrossRef\]](#)
22. Gómez-Ramírez, A.; Cotrino, J.; Lambert, R.M.; González-Elipé, A.R. Efficient Synthesis of Ammonia from N<sub>2</sub> and H<sub>2</sub> Alone in a Ferroelectric Packed-Bed DBD Reactor. *Plasma Sources Sci. Technol.* **2015**, *24*, 065011. [\[CrossRef\]](#)
23. Navascués, P.; Garrido-García, J.; Cotrino, J.; González-Elipé, A.R.; Gómez-Ramírez, A. Incorporation of a Metal Catalyst for the Ammonia Synthesis in a Ferroelectric Packed-Bed Plasma Reactor: Does It Really Matter? *ACS Sustain. Chem. Eng.* **2023**, *11*, 3621–3632. [\[CrossRef\]](#) [\[PubMed\]](#)
24. Xie, Q.; Zhuge, S.; Song, X.; Lu, M.; Yu, F.; Ruan, R.; Nie, Y. Non-Thermal Atmospheric Plasma Synthesis of Ammonia in a DBD Reactor Packed with Various Catalysts. *J. Phys. D Appl. Phys.* **2019**, *53*, 064002. [\[CrossRef\]](#)
25. Yaala, M.B.; Scherrer, D.-F.; Saeedi, A.; Moser, L.; Soni, K.; Steiner, R.; Temmerman, G.D.; Oberkofler, M.; Marot, L.; Meyer, E. Plasma-Activated Catalytic Formation of Ammonia from N<sub>2</sub>-H<sub>2</sub>: Influence of Temperature and Noble Gas Addition. *Nucl. Fusion* **2019**, *60*, 016026. [\[CrossRef\]](#)

26. Liu, J.; Zhu, X.; Hu, X.; Zhang, F.; Tu, X. Plasma-Assisted Ammonia Synthesis in a Packed-Bed Dielectric Barrier Discharge Reactor: Effect of Argon Addition. *Vacuum* **2022**, *197*, 110786. [[CrossRef](#)]
27. Patil, B.S.; van Kaathoven, A.S.R.; Peeters, F.J.J.; Cherkasov, N.; Lang, J.; Wang, Q.; Hessel, V. Deciphering the Synergy between Plasma and Catalyst Support for Ammonia Synthesis in a Packed Dielectric Barrier Discharge Reactor. *J. Phys. D Appl. Phys.* **2020**, *53*, 144003. [[CrossRef](#)]
28. Zhou, R.; Zhou, D.; Liu, B.; Nie, L.; Xian, Y.; Zhang, T.; Zhou, R.; Lu, X.; Ostrikov, K.K.; Cullen, P.J. Controlling Energy Transfer in Plasma-Driven Ammonia Synthesis by Adding Helium Gas. *ACS Sustain. Chem. Eng.* **2023**, *11*, 1828–1836. [[CrossRef](#)]
29. Li, Y.; Qin, L.; Wang, H.-L.; Li, S.-S.; Yuan, H.; Yang, D.-Z. High Efficiency NO<sub>x</sub> Synthesis and Regulation Using Dielectric Barrier Discharge in the Needle Array Packed Bed Reactor. *Chem. Eng. J.* **2023**, *461*, 141922. [[CrossRef](#)]
30. Hagelaar, G.; Pitchford, L. Solving the Boltzmann Equation to Obtain Electron Transport Coefficients and Rate Coefficients for Fluid Models. *Plasma Sources Sci. Technol.* **2005**, *14*, 722. [[CrossRef](#)]
31. Li, S.; van Raak, T.; Gallucci, F. Investigating the Operation Parameters for Ammonia Synthesis in Dielectric Barrier Discharge Reactors. *J. Phys. D Appl. Phys.* **2019**, *53*, 014008. [[CrossRef](#)]
32. Zhang, Y.; Li, J.; Lu, N.; Shang, K.; Mizuno, A.; Wu, Y. Evaluation of Discharge Uniformity and Area in Surface Dielectric Barrier Discharge at Atmospheric Pressure. *Vacuum* **2016**, *123*, 49–53. [[CrossRef](#)]
33. Liu, Y.; Wang, C.-W.; Xu, X.-F.; Liu, B.-W.; Zhang, G.-M.; Liu, Z.-W.; Chen, Q.; Zhang, H.-B. Synergistic Effect of Co-Ni Bimetal on Plasma Catalytic Ammonia Synthesis. *Plasma Chem. Plasma Process.* **2022**, *42*, 267–282. [[CrossRef](#)]
34. Wang, X.; Du, X.; Chen, K.; Zheng, Z.; Liu, Y.; Shen, X.; Hu, C. Predicting the Ammonia Synthesis Performance of Plasma Catalysis Using an Artificial Neural Network Model. *ACS Sustain. Chem. Eng.* **2023**, *11*, 4543–4554. [[CrossRef](#)]
35. Peng, P.; Li, Y.; Cheng, Y.; Deng, S.; Chen, P.; Ruan, R. Atmospheric Pressure Ammonia Synthesis Using Non-Thermal Plasma Assisted Catalysis. *Plasma Chem. Plasma Process.* **2016**, *36*, 1201–1210. [[CrossRef](#)]
36. Kim, H.-H.; Teramoto, Y.; Ogata, A.; Takagi, H.; Nanba, T. Atmospheric-Pressure Nonthermal Plasma Synthesis of Ammonia over Ruthenium Catalysts. *Plasma Process. Polym.* **2017**, *14*, 1600157. [[CrossRef](#)]
37. Hong, J.; Aramesh, M.; Shimoni, O.; Seo, D.H.; Yick, S.; Greig, A.; Charles, C.; Praver, S.; Murphy, A.B. Plasma Catalytic Synthesis of Ammonia Using Functionalized-Carbon Coatings in an Atmospheric-Pressure Non-Equilibrium Discharge. *Plasma Chem. Plasma Process.* **2016**, *36*, 917–940. [[CrossRef](#)]
38. Qayyum, A.; Zeb, S.; Naveed, M.A.; Rehman, N.U.; Ghauri, S.A.; Zakaullah, M. Optical Emission Spectroscopy of Ar–N<sub>2</sub> Mixture Plasma. *J. Quant. Spectrosc. Radiat. Transf.* **2007**, *107*, 361–371. [[CrossRef](#)]
39. Zhang, S.; Zong, L.; Zeng, X.; Zhou, R.; Liu, Y.; Zhang, C.; Pan, J.; Cullen, P.J.; Ostrikov, K.; Shao, T. Sustainable Nitrogen Fixation with Nanosecond Pulsed Spark Discharges: Insights into Free-Radical-Chain Reactions. *Green Chem.* **2022**, *24*, 1534–1544. [[CrossRef](#)]
40. Abdel-kader, M.E.; Gaber, W.H.; Ebrahim, F.A.; Abd Al-Halim, M.A. Characterization of the Electrical Breakdown for DC Discharge in Ar-He Gas Mixture. *Vacuum* **2019**, *169*, 108922. [[CrossRef](#)]
41. Brand, K.P. Dielectric Strength, Boiling Point and Toxicity of Gases—Different Aspects of the Same Basic Molecular Properties. *IEEE Trans. Electr. Insul.* **1982**, *17*, 451–456. [[CrossRef](#)]
42. Li, S.-Z.; Zhang, X.; Chen, C.-J.; Zhang, J.; Wang, Y.-X.; Xia, G.-Q. The Quenching Effect of Hydrogen on the Nitrogen in Metastable State in Atmospheric-Pressure N<sub>2</sub>-H<sub>2</sub> Microwave Plasma Torch. *Phys. Plasmas* **2014**, *21*, 073513. [[CrossRef](#)]
43. Hu, X.; Zhu, X.; Wu, X.; Cai, Y.; Tu, X. Plasma-Enhanced NH<sub>3</sub> Synthesis over Activated Carbon-Based Catalysts: Effect of Active Metal Phase. *Plasma Process. Polym.* **2020**, *17*, 2000072. [[CrossRef](#)]
44. Kosarev, I.N.; Khorunzhenko, V.I.; Mintoussov, E.I.; Sagulenko, P.N.; Popov, N.A.; Starikovskaia, S.M. A Nanosecond Surface Dielectric Barrier Discharge at Elevated Pressures: Time-Resolved Electric Field and Efficiency of Initiation of Combustion. *Plasma Sources Sci. Technol.* **2012**, *21*, 045012. [[CrossRef](#)]
45. Wang, Q.; Wu, H.; Wang, Y.; Zhang, Y.; Jiang, W.; Zhang, Y. Influence of Pulse Width on the Breakdown Process of Nanosecond Pulse Discharge at Low Pressure. *J. Phys. D Appl. Phys.* **2023**, *56*, 465201. [[CrossRef](#)]
46. Sun, J.; Chen, Q.; Zhao, X.; Lin, H.; Qin, W. Kinetic Investigation of Plasma Catalytic Synthesis of Ammonia: Insights into the Role of Excited States and Plasma-Enhanced Surface Chemistry. *Plasma Sources Sci. Technol.* **2022**, *31*, 094009. [[CrossRef](#)]
47. Qian, M.; Li, G.; Liu, S.; Zhang, Y.; Li, S.; Lin, Z.; Wang, D. Effect of Pulse Voltage Rising Time on Discharge Characteristics of a Helium–Air Plasma at Atmospheric Pressure. *Plasma Sci. Technol.* **2017**, *19*, 064015. [[CrossRef](#)]
48. Nakajima, J.; Sekiguchi, H. Synthesis of Ammonia Using Microwave Discharge at Atmospheric Pressure. *Thin Solid Film.* **2008**, *516*, 4446–4451. [[CrossRef](#)]
49. Luo, S.; Denning, C.M.; Scharer, J.E. Laser-Rf Creation and Diagnostics of Seeded Atmospheric Pressure Air and Nitrogen Plasmas. *J. Appl. Phys.* **2008**, *104*, 013301. [[CrossRef](#)]
50. Wang, Y.; Craven, M.; Yu, X.; Ding, J.; Bryant, P.; Huang, J.; Tu, X. Plasma-Enhanced Catalytic Synthesis of Ammonia over a Ni/Al<sub>2</sub>O<sub>3</sub> Catalyst at Near-Room Temperature: Insights into the Importance of the Catalyst Surface on the Reaction Mechanism. *ACS Catal.* **2019**, *9*, 10780–10793. [[CrossRef](#)] [[PubMed](#)]
51. Hong, J.; Pancheshnyi, S.; Tam, E.; Lowke, J.J.; Praver, S.; Murphy, A.B. Kinetic Modelling of NH<sub>3</sub> Production in N<sub>2</sub>-H<sub>2</sub> Non-Equilibrium Atmospheric-Pressure Plasma Catalysis. *J. Phys. D Appl. Phys.* **2017**, *50*, 154005. [[CrossRef](#)]
52. Wang, L.; Yi, Y.; Zhao, Y.; Zhang, R.; Zhang, J.; Guo, H. NH<sub>3</sub> Decomposition for H<sub>2</sub> Generation: Effects of Cheap Metals and Supports on Plasma–Catalyst Synergy. *ACS Catal.* **2015**, *5*, 4167–4174. [[CrossRef](#)]

53. Zhang, T.; Zhou, R.; Zhang, S.; Zhou, R.; Ding, J.; Li, F.; Hong, J.; Dou, L.; Shao, T.; Murphy, A.B.; et al. Sustainable Ammonia Synthesis from Nitrogen and Water by One-Step Plasma Catalysis. *Energy Environ. Mater.* **2023**, *6*, e12344. [[CrossRef](#)]
54. Hong, J.; Praver, S.; Murphy, A.B. Production of Ammonia by Heterogeneous Catalysis in a Packed-Bed Dielectric-Barrier Discharge: Influence of Argon Addition and Voltage. *IEEE Trans. Plasma Sci.* **2014**, *42*, 2338–2339. [[CrossRef](#)]
55. Sode, M.; Jacob, W.; Schwarz-Selinger, T.; Kersten, H. Measurement and Modeling of Neutral, Radical, and Ion Densities in H<sub>2</sub>-N<sub>2</sub>-Ar Plasmas. *J. Appl. Phys.* **2015**, *117*, 083303. [[CrossRef](#)]

**Disclaimer/Publisher’s Note:** The statements, opinions and data contained in all publications are solely those of the individual author(s) and contributor(s) and not of MDPI and/or the editor(s). MDPI and/or the editor(s) disclaim responsibility for any injury to people or property resulting from any ideas, methods, instructions or products referred to in the content.